
Directional compact hexahedral loudspeaker array

Yuyao YUAN

Yuyao.Yuan.Etu@univ-lemans.fr

Yuyang LIU

Yuyang.Liu.Etu@univ-lemans.fr

Supervisor : Bruno GAZENGEL
Antonin NOVAK

Le Mans Université

International Master's Degree in ElectroAcoustics

11 June 2023

Abstract

In systems where multiple speakers are tightly integrated, the reproduction of a sound field with multi-directionality becomes possible. Compact polyhedral loudspeaker arrays, equipped with multiple drive units, offer the potential to generate complex sound fields by independently controlling the voltage of each speaker. This project aims to manufacture and elucidate the workings of a specific type of powerful loudspeaker array known as the compact hexahedral loudspeaker array. The research will focus on understanding its electromechanical characteristics, the principles behind its radiation patterns, and the utilization of different input configurations for sound beam control.

Acknowledgment

We would like to acknowledge and express our gratitude to all those who supported and assisted us during this research project. Special thanks to Mr. Bruno Gazengel for his guidance in creating the electromechanical model, to Mr. Antonin Novak for his guidance in setting up the DSP throughout the study, and to Mr. Alann Renault for his help to create the prototype.

We are also grateful to all members of the M1 IMDEA class. We finally thank ourselves and our teammates who have been working hard throughout the process and who have accompanied and encouraged each other.

Contents

I Introduction	1
II Literature review	1
III System Description	2
III.1 Prototype	2
III.2 Sound chain	3
III.3 Thiele & Small parameter estimation	3
IV Theoretical Framework	4
IV.1 Electromechanical modeling	4
IV.2 Radiated pressure field	7
IV.3 3D first-order beam control	8
IV.3.1 Principle of 3D first-order beam control	8
IV.3.2 Monopole - dipole equalization	10
V Simulation & Experimental Result Analysis	11
V.1 Electromechanical behavior	11
V.2 Validity of Heq	14
V.3 Realization of 3D first-order beam control	15
V.3.1 Implement and DSP	16
V.3.2 Experimental setup	17
V.3.3 Experimental results & Analysis	18
VI Conclusion	21
Appendix	22
A Speaker Datasheet	22
B Thiele & Small Parameters	23
C Derivation of the pressure expression in two dimention	23
D Green's function + Integral formalism method	24

I Introduction

In recent years, there has been a growing interest in the field of auditory effect, where a good sound system is not only able to create an immersive soundscape, but also enhance the overall sensory experience. The design and study of loudspeaker arrays have been an active area of research for several decades, aimed at achieving 3D audio systems and reproducing specific sound fields. Loudspeaker arrays typically comprise multiple loudspeakers placed around the listener, leveraging the acoustic properties of the environment to create a surround sound effect. Compact loudspeaker arrays, on the other hand, consists of a series of transducers embedded in a spherical or polyhedral cabinet. Unlike conventional decentralized loudspeaker arrays, compact loudspeaker arrays can be considered as a single complex source, capable of producing multiple patterns of directional radiation.

Compact loudspeaker arrays have been shown to have diverse applications. For instance, when the array's drive units are driven identically, it can serve as an approximate omnidirectional source for room acoustic measurements, such as impulse response measurements in enclosed spaces. On the other hand, when separate power supplies are used to independently control each loudspeaker, the array can be used as a directional source to produce any sound field or reproduce the sound field without interaction problems with the surrounding environment. Moreover, compact loudspeaker arrays have demonstrated the potential to achieve active control of sound.

The purpose of this study is to establish and study the electromechanical characteristics and acoustic radiation field of a compact hexahedral loudspeaker array. And to realize the 3D first-order beam control of the loudspeaker array based on the 3D first-order Ambisonics recording and playback technique.

II Literature review

Since 2001, when the compact loudspeaker **La Timée** of the IRCAM laboratory was created, many acousticians and engineers have devoted themselves to the exploration of the characteristics and applications of compact polyhedral loudspeaker arrays.

The article published by A. M. Pasqual et al. in 2010 describes two methods for building an electromechanical model of a compact spherical loudspeaker array with a common enclosure [1]. The present work further improves the electromechanical model of the cubic hexahedral loudspeaker array. Meanwhile, A.M. Pasqual studied the omnidirectional acoustic radiation model of compact loudspeaker arrays based on Platonic solid [2], which provided ideas for the conversion from membrane vibration velocity to pressure field in this study. This article also compared the properties of the loudspeaker array in different platonic solid shapes. The results demonstrated that the dodecahedral array layout is superior, while hexahedra or tetrahedra could be used as viable alternatives when the number of loudspeakers was less than twelve. In 2018, T. Deppisch et al implemented a two-dimensional first-order sound beam control using a hexahedral loudspeaker array with 4 loudspeakers in the horizontal facet [3]. It gives the process from the input voltage to achieve directional control, which serves as a specification for the project arrangement. Finally, based on the interpretation of the Ambisonics technique by F. Zotter and M. Frank [4], first-order 3D beam control was implemented.

III System Description

This study details the design, construction, and acoustic analysis of a compact hexahedral loudspeaker array consisting of six identical drivers mounted in a square plywood enclosure. This section provides an overview of the system's design sketches, physical parameters, and sound chain design.

III.1 Prototype

The loudspeaker array is composed of three primary components: six Visaton FR 13 - 4 ohm full-range drivers, a plywood cube enclosure, and a stand. Figure 1 shows a photograph of the constructed prototype of the hexahedral loudspeaker array.

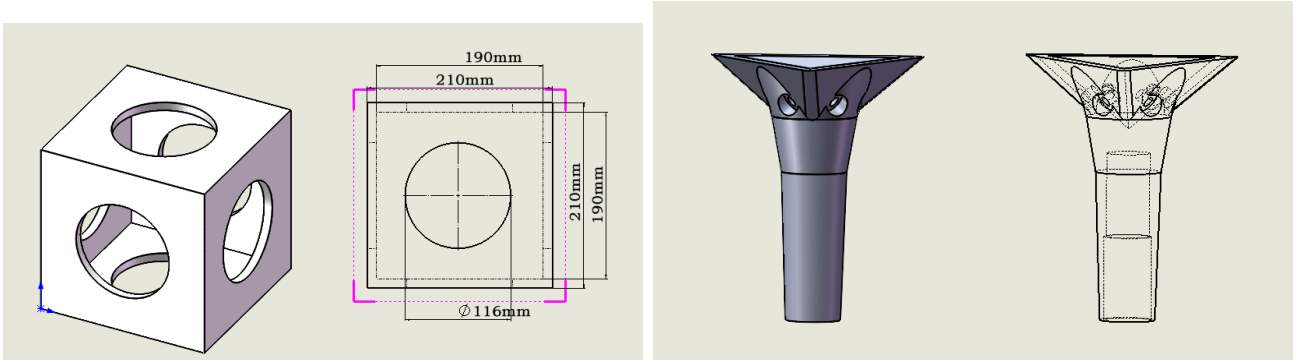


Figure 1: Hexahedral loudspeaker array prototype with 6 transducers mounted on a hollow hexahedral cavity.

The prototype comprises six Visaton FR 13 - 4 ohm full-range drivers with an effective vibrating surface of 87 cm^2 and a thickness of 43 cm, which allows for a higher ratio of effective diaphragm area to baffle area while taking up less volume internally. These drivers possess a bandwidth of [65,20000] Hz. Its full coverage frequency range guarantees excellent bandwidth for the hexahedral speaker array. For more detailed information about these drivers, please refer to their datasheet, provided in Appendix A.

The plywood cube enclosure is constructed using 10 mm thick plywood, which is cut and glued into a square hexahedron with interior dimensions of 19 cm and exterior dimensions of 21 cm. The sketch of the cavity is shown in Figure 2a. Its highly symmetrical structure ensures an even distribution of the sound field radiated by the loudspeakers in three dimensions. The internal cubic cavity of the enclosure simplifies the modeling of acoustic coupling between the loudspeakers. The enclosure dimensions used in the prototype also resulted in a system with a high ratio of effective diaphragm area to baffle area, which ensured good sound radiation efficiency while providing the space required for speaker and internal circuitry assembly.

To support the speaker and enclosure, a stand with a height of approximately 0.7 m is designed. A connector capable of holding a square hexahedron was 3D printed to connect the body of the system to a simple stand. Figure 2b shows the sketch of the designed connector. The stand also helps to reduce the impact of ground-reflected sound waves on the radiated sound field.



(a) Sketch of the designed enclosure for speakers. (b) Sketch of the connector to connect the loudspeaker to a bracket.

Figure 2: Sketch of the enclosure and the connector.

III.2 Sound chain

This project aims to investigate the possibility of achieving the 3D first-order directional radiated sound field. To accomplish this goal, independent control of each loudspeaker is necessary. Three Wondom AA-JA32172 2 x 50W@4Ohm two-channel amplifier boards with integrated digital signal processors are employed to achieve this independent control. The filter design for the different output channels of amplifiers enables individual control of each driver. Figure 3 presents the sound chain of this loudspeaker system. Furthermore, due to the volume constraints of the loudspeaker cavity, a separate box is utilized to accommodate the amplifiers and the source supply.

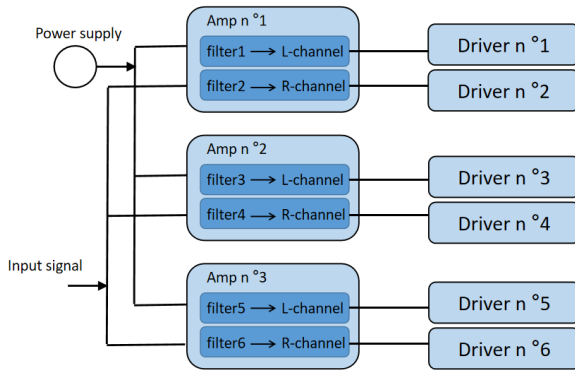


Figure 3: Sound chain of the system.

III.3 Thiele & Small parameter estimation

To ensure the accuracy of simulation results, it is crucial to obtain precise Thiele & Small (TS) parameters for each of the six electrodynamic loudspeakers used in the prototype. The experiments were carried out to estimate the TS parameters of the six drivers by the added mass method. The

measured and estimated electrical impedance and the estimated TS parameters are presented in Appendix B. The agreement between the measurement and estimation results at low frequencies indicates that the estimated TS parameters are accurate and that they provide a reliable characterization of the drivers, and they are important for accurately modeling the behavior of the loudspeakers in simulations.

IV Theoretical Framework

This section aims to present the working principle of a compact hexahedral loudspeaker array. Firstly, the system's electromechanical model is established by considering the characteristics of the loudspeakers themselves. By using transmission lines and acoustic theory, the acoustic coupling problem caused by the shared enclosure is solved, so that the relationship between the input voltage and the vibration velocity of the diaphragm is established. Subsequently, the radiated acoustic field of the whole system is synthesized using the spherical harmonic function. Finally, the input voltage required to achieve directivity control in the system is derived based on an understanding of the three-dimensional first-order Ambisonics technique.

IV.1 Electromechanical modeling

The six electrodynamic loudspeakers of the system are numbered 1-6. The working situation of each loudspeaker can be divided into electrical, mechanical, and acoustic parts. All three components can be transformed into the mechanical domain based on the motion equation of each loudspeaker's membrane. It is assumed that the membranes are rigid bodies, which means that all points on the membrane vibrate uniformly and all speakers have the same S membrane area.

For the l th loudspeaker, its input variable is the voltage U_l fed to its coil, and the output variable is the velocity v_l of the membrane. Under the convention $e^{j\omega t}$, its motion equation with harmonic signal in the frequency domain can be represented as the Equation (1), where M_{msl} , R_{msl} , C_{msl} , B_l and Z_{el} are independent Thiele-Small parameters concerning the particular loudspeaker obtained before; F_{al} is the force caused by the sound pressure of the membrane vibrations of all loudspeakers in the system.

$$(j\omega M_{msl} + R_{msl} + \frac{1}{j\omega C_{msl}})v_l = F_{al} + \frac{B_l}{Z_{el}}(U_l - B_l v_l). \quad (1)$$

The expression of the force F_{al} reflects the acoustic coupling between the loudspeakers and the enclosure. It is related to the acoustic pressure from the l' speaker to the l speaker $p_{ll'}$, which can be expressed as a function of the volume velocity provided by the operating driver and the resulting external and internal acoustic impedance of the observation driver. The force received by the l th loudspeaker can be obtained as a summation, as shown in Equation (2), where $Z_{ll'}^-$ and $Z_{ll'}^+$ represent the magnitude of the internal and external acoustic impedance, respectively; S is the effective membrane area of the speaker.

$$F_{al} = \sum_{l'=1}^6 F_{al'l'} = S \sum_{l'=1}^6 p_{ll'} = S \sum_{l'=1}^6 (-Z_{ll'}^- - Z_{ll'}^+) v_{l'} S. \quad (2)$$

Combining the motion equations of all six loudspeakers, the electromechanical behavior of the whole system can use a six-order vector formula to express, which is the formula (3), where the independent parameters can form diagonal matrices and the impedance matrices are not diagonal due to acoustic coupling. By simplifying the notation, the global expression is represented by equation (4).

$$\left(j\omega \mathbf{M}_{ms} + \mathbf{R}_{ms} + \frac{\mathbf{C}_{ms}^{-1}}{j\omega} + \mathbf{B}\mathbf{l}^2\mathbf{Z}_e^{-1} \right) \vec{v} + \mathbf{S} (\mathbf{Z}^- + \mathbf{Z}^+) \mathbf{S} \vec{v} = \mathbf{B}\mathbf{l}\mathbf{Z}_e^{-1} \vec{U}. \quad (3)$$

$$\mathbf{G}\vec{v} + \mathbf{S} (\mathbf{Z}^- + \mathbf{Z}^+) \mathbf{S} \vec{v} = \mathbf{B}\vec{U}. \quad (4)$$

Matrices \mathbf{G} , \mathbf{S} , and \mathbf{B} are composed of the simulated TS parameters obtained in Appendix B. It is assumed that the system is placed in an infinite space, and the external acoustic radiation impedance is negligible compared to the internal acoustic impedance. For the internal impedance Z^- , the first method is based on Green's function method, which is expanded in Appendix D. The second method is derived by using the knowledge of transmission lines and acoustic analysis. In this method, the direct view of the system sketch is shown in Figure 4. Two active loudspeakers face each other. The 4 other loudspeakers are passive radiators with an area of S . Here assuming that the two active loudspeakers are drivers 1 and 2.

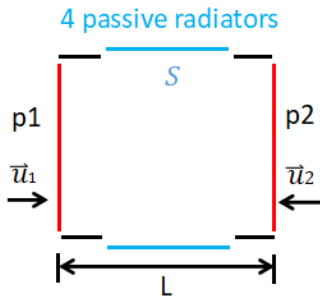


Figure 4: Direct view of the sketch of the system for one dimension propagation problem

At first, only the 1D problem is studied. The passive radiators are considered rigid bodies ($\vec{v}_i = 0$, $i = 3, 4, 6$). According to the knowledge of transmission lines [5], the expression of the impedance matrix is Equation (5), where $Z_c = \frac{\rho c}{S_0}$ is acoustic impedance and $S_0 = L^2$ is the whole surface area.

$$\begin{pmatrix} p_1 \\ p_2 \end{pmatrix} = \begin{pmatrix} -jZ_c \cot(kL) & -\frac{jZ_c}{\sin(kL)} \\ \frac{-jZ_c}{\sin(kL)} & -jZ_c \cot(kL) \end{pmatrix} \begin{pmatrix} v_1 S \\ v_2 S \end{pmatrix} \quad (5)$$

The Taylor expansion in the low-frequency range for $-jZ_c \cot(kL)$ and $-jZ_c \frac{1}{\sin(kL)} = -jZ_c \csc(kL)$ are Equation (6) and (7), respectively (keep terms until the first order).

$$-jZ_c \cot(kL) = \frac{1}{j} \frac{\rho c}{S_0} \left(\frac{1}{kL} - \frac{kL}{3} \right) = \frac{\rho c^2}{j\omega L S_0} + j\omega \frac{\rho L}{3 S_0} \quad (6)$$

$$-jZ_c \csc(kL) = \frac{1}{j} \frac{\rho c}{S_0} \left(\frac{1}{kL} + \frac{kL}{6} \right) = \frac{\rho c^2}{j\omega L S_0} - j\omega \frac{\rho L}{6 S_0} \quad (7)$$

In lumped element method, $\frac{\rho c^2}{j\omega LS_0} = \frac{\rho c^2}{j\omega V}$ can be considered as acoustic compliance $Z_C = \frac{1}{j\omega C_a}$, and $j\omega \frac{\rho L}{S_0}$ is acoustic mass $Z_M = j\omega M_a$. The impedance matrix of the first step is Equation (8).

$$\begin{pmatrix} p_1 \\ p_2 \end{pmatrix} = \begin{pmatrix} \frac{1}{j\omega C_a} + j\omega \frac{M_a}{3} & \frac{1}{j\omega C_a} - j\omega \frac{M_a}{6} \\ \frac{1}{j\omega C_a} - j\omega \frac{M_a}{6} & \frac{1}{j\omega C_a} + j\omega \frac{M_a}{3} \end{pmatrix} \begin{pmatrix} v_1 S \\ v_2 S \end{pmatrix} = \begin{pmatrix} Z_C + \frac{Z_M}{3} & Z_C - \frac{Z_M}{6} \\ Z_C - \frac{Z_M}{6} & Z_C + \frac{Z_M}{3} \end{pmatrix} \begin{pmatrix} v_1 S \\ v_2 S \end{pmatrix} \quad (8)$$

The second step is to take into account the effect of the 4 passive radiators. Now the problem should be extended to three dimensions. Thanks to the symmetry of the system, the conclusion can be obtained from the two-dimensional problem: the pressure p_1 caused by the 2 adjacent loudspeakers. The prototype is represented in Figure 5. The moving membranes 3 and 4 can be seen as moving pistons with area $S_m = L^2$.

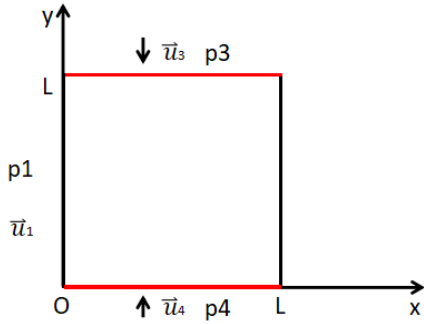


Figure 5: Direct view of the sketch of the system for two dimension propagation problem

With the 2D propagation problem in harmonic and the boundary conditions $\vec{v}|_{x=0} = \vec{v}|_{x=L} = 0$, the pressure field of this system can be derived. The precise derivation is in Appendix C. The first cut-off frequency f_1 corresponds to the solution of $k_{x_1} = \frac{\pi}{L}$ when there are only propagating waves in the y-axis. The value of f_1 is 900 Hz. The expression of the acoustic pressure at the center of the membrane of the first loudspeaker with $f \leq f_1$ is shown in Equation (9).

$$p_1(\frac{L}{2}, \omega) = -\frac{jZ_c}{2} \csc(\frac{kL}{2}) v_3 S - \frac{jZ_c}{2} \csc(\frac{kL}{2}) v_4 S = (Z_C - \frac{Z_M}{24}) v_3 S + (Z_C - \frac{Z_M}{24}) v_4 S. \quad (9)$$

The final matrix now can be created. It is assumed that drivers 1,2, drivers 3,4, and drivers 5,6 are three face-to-face loudspeaker groups. The pressure function with the final internal impedance matrix Z^- is Equation (10).

$$\begin{pmatrix} p_1 \\ p_2 \\ p_3 \\ p_4 \\ p_5 \\ p_6 \end{pmatrix} = \begin{pmatrix} Z_C + \frac{Z_M}{3} & Z_C - \frac{Z_M}{6} & Z_C - \frac{Z_M}{24} & Z_C - \frac{Z_M}{24} & Z_C - \frac{Z_M}{24} & Z_C - \frac{Z_M}{24} \\ Z_C - \frac{Z_M}{6} & Z_C + \frac{Z_M}{3} & Z_C - \frac{Z_M}{24} & Z_C - \frac{Z_M}{24} & Z_C - \frac{Z_M}{24} & Z_C - \frac{Z_M}{24} \\ Z_C - \frac{Z_M}{24} & Z_C - \frac{Z_M}{24} & Z_C + \frac{Z_M}{3} & Z_C - \frac{Z_M}{6} & Z_C - \frac{Z_M}{24} & Z_C - \frac{Z_M}{24} \\ Z_C - \frac{Z_M}{24} & Z_C - \frac{Z_M}{24} & Z_C - \frac{Z_M}{6} & Z_C + \frac{Z_M}{3} & Z_C - \frac{Z_M}{24} & Z_C - \frac{Z_M}{24} \\ Z_C - \frac{Z_M}{24} & Z_C - \frac{Z_M}{24} & Z_C - \frac{Z_M}{24} & Z_C - \frac{Z_M}{24} & Z_C + \frac{Z_M}{3} & Z_C - \frac{Z_M}{6} \\ Z_C - \frac{Z_M}{24} & Z_C - \frac{Z_M}{24} & Z_C - \frac{Z_M}{24} & Z_C - \frac{Z_M}{24} & Z_C - \frac{Z_M}{6} & Z_C + \frac{Z_M}{3} \end{pmatrix} \begin{pmatrix} v_1 S \\ v_2 S \\ v_3 S \\ v_4 S \\ v_5 S \\ v_6 S \end{pmatrix} \quad (10)$$

After preparing all the elements of the vector formula, the velocities of the membranes are represented in Equation 11. Depending on the input configurations, the dynamic properties of the entire system will vary.

$$\vec{v} = (\mathbf{G} + \mathbf{S} \mathbf{Z}^- \mathbf{S})^{-1} \times \mathbf{B} \vec{U}. \quad (11)$$

IV.2 Radiated pressure field

Knowing the vibration velocity of the membrane allows the construction of the radiated sound field of the system. Based on the research of A. M. Pasqual in 2014 [2], the ortho-hexahedral loudspeaker array system can be seen as a Platonic solid. Since usually the membrane of a loudspeaker is conical or dome-shaped, when the membrane is working bulging it can be seen as the cap of the external tangent sphere of the hexahedron, the most ideal geometric working model is represented in Figure 6. The ratio of the vibrating membrane area to the surface area is usually smaller.

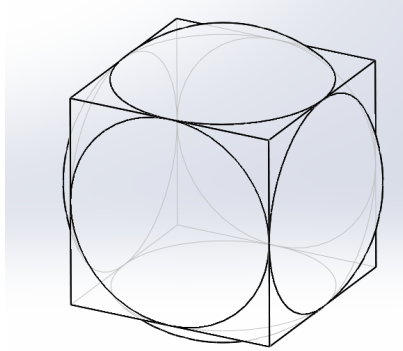


Figure 6: Hexahedral Platonic solid and its tangent sphere - an ideal dynamic model of a hexahedral loudspeaker array working with membranes

In the near-field system surface, the vibration of the membrane drives the vibration of the surrounding air. Here it is assumed that the velocity of the gas distributed on the surface of the tangent sphere is equal to the velocity of the membrane of its adjacent loudspeaker. If the radius of the tangent sphere is r_0 , then the velocity at any point (θ, ϕ) on its surface can be written in the form of a spherical harmonic series as Equation (12), where θ is the polar angle in $[0, \pi]$ and ϕ is the azimuth in $[0, 2\pi]$; $Y_m^n(\theta, \phi)$ are the spherical harmonics whose expression is Equation (13), where $P_n^m(\cdot)$ is the Legendre function of the first kind; $V_{mn}(r_0)$ corresponds to the coefficients of Y_m^n .

$$v(r_0, \theta, \phi) = \sum_{n=0}^N \sum_{m=-n}^n V_{mn}(r_0) Y_m^n(\theta, \phi). \quad (12)$$

$$Y_m^n(\theta, \phi) = (-1)^m \sqrt{\frac{(2n+1)}{4\pi} \frac{(n-m)!}{(n+m)!}} P_n^m(\cos\theta) e^{im\phi}. \quad (13)$$

Similarly, the far-field radiated sound pressure of the system on the surface of a sphere of radius r can also be expressed as a spherical harmonic series as Equation (14). At the same spherical harmonic, the sound pressure coefficient $P_{mn}(r)$ and the sound velocity coefficient $V_{mn}(r_0)$ can be found by the Euler equation. According to the wave propagation equation in the spherical coordinate system, when its boundary condition is a rigid wall at r_0 and the propagation region is $r \geq r_0$, its propagation equation is of the nth order second type of Hankel equation $h_n^{(2)}(kr)$. The relation expression between $P_{mn}(r)$ and $V_{mn}(r_0)$ is represented in Equation (15).

$$p(r, \theta, \phi) = \sum_{n=0}^N \sum_{m=-n}^n P_{mn}(r) Y_m^n(\theta, \phi). \quad (14)$$

$$P_{mn}(r) = -i\rho c \frac{h_n^{(2)}(kr)}{h_n'^{(2)}(kr_0)} V_{mn}(r_0). \quad (15)$$

The value of $V_{mn}(a)$ can be obtained by the decomposition of the spherical harmonic series as Equation (16). The process can be analogous to the decomposition of the Fourier series, but the variables are the angles θ and ϕ .

$$V_{mn}(r_0) = \int_0^\pi \int_0^{2\pi} v(r_0, \theta, \phi) Y_n^{m*}(\theta, \phi) \sin \theta d\phi d\theta. \quad (16)$$

According to the description of the system geometry at the beginning of this section, the range of integration is the coverage of the membrane of the loudspeaker. The result of the integration is expressed in Equation 17, which corresponds to the moving velocities of all loudspeakers of the system. Here (θ_l, ϕ_l) are associated with the coordinates of the center of the membrane of the l th loudspeaker; the angle θ_0 represents the included angle between the line connecting the center of the outer tangent sphere to the center of the speaker membrane and the line connecting the center of the sphere to the edge of the membrane. Here θ_0 is 29.26° . Using this expression to replace $V_{mn}(r_0)$ in Equation (15), the radiation pressure field formula can be obtained.

$$V_{mn} = \frac{2\pi}{2n+1} (P_{n-1}(\cos \theta_0) - P_{n+1}(\cos(\theta_0))) \sum_{l=1}^6 v_l Y_n^{m*}(\theta_l, \phi_l). \quad (17)$$

IV.3 3D first-order beam control

IV.3.1 Principle of 3D first-order beam control

3D first-order beam control is achieved by superimposing a weighted omnidirectional pattern signal and three orthogonal figure-of-eight pattern signals. These four channel signals are decoded to the loudspeakers to achieve control of the arbitrary aiming direction of the radiated sound field of the loudspeaker array in 3D space. This principle is based on the 3D first-order Ambisonics recording and playback technology.

In the 2D plane, the 1st-order directivity pattern is expressed as:

$$D(\phi) = 1 - \alpha + \alpha \cos(\phi - \phi_0), \quad (18)$$

where the independent variable is the azimuth ϕ , and the aiming direction is ϕ_0 . The directivity shape is controlled by the value of α , which varies from 0 to 1. One can get omnidirectional ($\alpha = 0$), cardioid($\alpha = \frac{1}{2}$), supercardioid($\alpha = \frac{2}{3}$), figure-of-eight($\alpha = 1$), or any shape between 2 directivity patterns.

The Equation (18) can also be expressed as:

$$D(\phi) = 1 - \alpha + \alpha \cos(\phi_0) \cos(\phi) + \alpha \sin(\phi_0) \sin(\phi). \quad (19)$$

which can be considered as a superposition of an omnidirectional pattern and two figure-of-eight patterns aligned with the orthogonal axes, respectively. Their weights can be denoted by W, X, and Y, respectively, which depend on the directivity shape parameter α and the aiming direction ϕ_0 .

In Equation (19), for the first-order directivity pattern, the first term represents the omnidirectional pattern weighted by $W = 1 - \alpha$. The second term represents the figure-of-eight pattern aligned with the x-axis in the Cartesian coordinate system weighted by $X = \alpha \cos(\phi_0)$, where $\cos(\phi_0)$ is the cosine of the included angle between the direction ϕ_0 and the x-axis. Similarly, the third term represents the figure-of-eight pattern aligned with the y-axis and weighted by $Y = \alpha \sin(\phi_0)$, where $\sin(\phi_0) = \cos(\phi_0 - \frac{\pi}{2})$ is the cosine of the included angle of the direction θ_0 and the y-axis.

In 3D space, one can no longer determine the direction only by azimuth; the polar angle must also be taken into account. For this purpose, the direction vector $\vec{\Phi}$ is introduced. The direction vector is of unit length $\|\vec{\Phi}\| = 1$, and is expressed in the spherical coordinate system as:

$$\vec{\Phi} = \begin{pmatrix} \sin(\theta) \cos(\varphi) \\ \sin(\theta) \sin(\varphi) \\ \cos(\theta) \end{pmatrix}, \quad (20)$$

where θ and ϕ denote the polar angle and azimuth in the spherical coordinate system, respectively. The inner product $\vec{\Phi}_1^T \vec{\Phi}_2$ of two direction vectors corresponds to the cosine of their included angle.

The directivity pattern with aiming direction $\vec{\Phi}_0$ in 3D space is expressed as:

$$D(\vec{\Phi}) = 1 - \alpha + \alpha \vec{\Phi}_0^T \vec{\Phi}. \quad (21)$$

Similar to the 2D plane, the pointing pattern in 3D space can be decomposed into an omnidirectional pattern and three figure-of-eight patterns along the x, y, and z axes, respectively. They are weighted as W, X, Y, and Z, respectively, and expressed as the following equation:

$$\begin{pmatrix} W \\ X \\ Y \\ Z \end{pmatrix} = \begin{pmatrix} 1 - \alpha \\ \alpha \vec{\Phi}_0^T \vec{\Phi}_x \\ \alpha \vec{\Phi}_0^T \vec{\Phi}_y \\ \alpha \vec{\Phi}_0^T \vec{\Phi}_z \end{pmatrix}, \quad (22)$$

here $\vec{\Phi}_0$ denotes the aiming direction, $\vec{\Phi}_x^T = [1, 0, 0]$, $\vec{\Phi}_y^T = [0, 1, 0]$, and $\vec{\Phi}_z^T = [0, 0, 1]$ are the direction vectors corresponding to the x, y, and z axes of the Cartesian coordinate system, respectively. Combined with Equation (20), these weights can be expressed as:

$$\begin{pmatrix} W \\ X \\ Y \\ Z \end{pmatrix} = \begin{pmatrix} 1 - \alpha \\ \alpha \sin(\theta_0) \cos(\varphi_0) \\ \alpha \sin(\theta_0) \sin(\varphi_0) \\ \alpha \cos(\theta_0) \end{pmatrix}, \quad (23)$$

where the pair of angles (θ_0, ϕ_0) represents the polar angle and the azimuth of the aiming direction in the spherical coordinate system.

After obtaining the expressions of W, X, Y, and Z, the continuous directivity pattern can be mapped to speakers in a loudspeaker array with an arbitrary layout by means of the 3d first-order Ambisonics sampling decoder matrix [4]. Knowing the direction vectors $\{\vec{\Phi}_l\}$ of a series of loudspeakers of a loudspeaker array and the unit direction vectors $\vec{\Phi}_x$, $\vec{\Phi}_y$ and $\vec{\Phi}_z$ corresponding to the x, y, and z axes, the loudspeaker signals can be determined by the following equation:

$$\begin{pmatrix} S_1 \\ \vdots \\ S_l \end{pmatrix} = \begin{pmatrix} 1 & \vec{\Phi}_1^T \vec{\Phi}_x & \vec{\Phi}_1^T \vec{\Phi}_y & \vec{\Phi}_1^T \vec{\Phi}_z \\ \vdots & & & \\ 1 & \vec{\Phi}_l^T \vec{\Phi}_x & \vec{\Phi}_l^T \vec{\Phi}_y & \vec{\Phi}_l^T \vec{\Phi}_z \end{pmatrix} \begin{pmatrix} W \\ X \\ Y \\ Z \end{pmatrix} s(t). \quad (24)$$

The input signal $s(t)$ is decomposed into a series of loudspeaker signals $\{S_l\}$ provided to the corresponding loudspeakers so that the radiated sound field of the loudspeaker array has a directivity shape corresponding to the value of α and an aiming direction (θ_0, ϕ_0) .

The prototype hexahedral loudspeaker array studied in the project consists of identical loudspeakers distributed in the centers of six faces. These six loudspeakers can be divided into three pairs: front and back, left and right, and top and bottom, whose axes are parallel to the x-axis, y-axis, and z-axis, respectively. These six speakers are denoted as S_{x+} , S_{x-} , S_{y+} , S_{y-} , S_{z+} , and S_{z-} . The transpose of their corresponding direction vectors are $\vec{\Phi}_{x+}^T = [1, 0, 0]$, $\vec{\Phi}_{x-}^T = [-1, 0, 0]$, $\vec{\Phi}_{y+}^T = [0, 1, 0]$, $\vec{\Phi}_{y-}^T = [0, -1, 0]$, $\vec{\Phi}_{z+}^T = [0, 0, 1]$, and $\vec{\Phi}_{z-}^T = [0, 0, -1]$, respectively.

Combining Equation (23) and Equation (24), the input signals of the six-speakers of the hexahedral speaker array can be calculated by the following equation:

$$\begin{pmatrix} S_{x+} \\ S_{x-} \\ S_{y+} \\ S_{y-} \\ S_{z+} \\ S_{z-} \end{pmatrix} = \begin{pmatrix} 1 & 1 & 0 & 0 \\ 1 & -1 & 0 & 0 \\ 1 & 0 & 1 & 0 \\ 1 & 0 & -1 & 0 \\ 1 & 0 & 0 & 1 \\ 1 & 0 & 0 & -1 \end{pmatrix} \begin{pmatrix} 1 - \alpha \\ \alpha \sin(\theta_0) \cos(\phi_0) \\ \alpha \sin(\theta_0) \sin(\phi_0) \\ \alpha \cos(\theta_0) \end{pmatrix} s(t). \quad (25)$$

From Equation (25), it can be concluded that the omnidirectional pattern is formed by all the speakers on the hexahedral loudspeaker acting together in phase, and the axial figure-of-eight pattern is formed by the corresponding pair of speakers acting out of phase. By setting the set value of α and the angle of the aiming direction (θ_0, ϕ_0) , the omnidirectional components and axial figure-of-eight components of the radiated sound field of the loudspeakers are weighted and superimposed to achieve the directivity control of the loudspeaker array.

IV.3.2 Monopole - dipole equalization

The 3D first-order beam control technique is based on the control of a linear combination of the omnidirectional (monopole) pattern and bidirectional (dipole) pattern. In order to finally achieve the directivity control of the sound field, the input signal needs to pass through the equalizer H_{eq} , which is designed to make the sound pressure ratio of the two modes at a point in the sound field the same as the input voltage ratio, i.e. $\frac{p_{monopole}}{p_{dipole}} = \frac{U_{monopole}}{U_{dipole}}$ [3]. H_{eq} is divided into two parts, the first part, H_{eq1} , is designed to equalize the difference between the membrane oscillation velocities due to the different acoustic coupling loads in the two modes. The second part, H_{eq2} , is designed to equalize the difference in the radiated sound pressure generated by the system in the two modes.

Both two equalizers are added to the monopole mode component of speaker signals. According to the analysis of the Section IV.1 and the expression of the velocity in Equation (11), the expression of the H_{eq1} of the l th loudspeaker is Equation (26).

$$H_{eq1_l} = \frac{v_{mono_l}}{v_{dip_l}} \frac{U_{dip_l}}{U_{mono_l}} = \frac{(G_l + S^2 6 Z_C)}{(G_l + S^2 \frac{Z_M}{6})}. \quad (26)$$

To solve for H_{eq2} , the system in two modes is considered as a monopole source or as a dipole source with the same radius r_0 , and with a surface vibrating at v_{mono} or v_{dip} , respectively. Based on the knowledge from the course on radiation elements [6], combined with the above boundary conditions, it is possible to find H_{eq2} at the distance r as shown in Equation (27), where $k = \frac{\omega}{c}$ is the onde number.

$$H_{eq2}(r) = \frac{p_{dip}}{p_{mono}} \frac{v_{mono}}{v_{dip}} = \frac{-\frac{e^{-ikr}}{4\pi r} (ik + \frac{1}{r})}{\frac{e^{-ikr}}{4\pi r}} \frac{-\frac{e^{-ikr}}{4\pi r} (ik + \frac{1}{r})}{\frac{e^{-ikr}}{4\pi r} \left[(ik + \frac{1}{r})^2 + \frac{1}{r^2} \right]} = \frac{(ik + \frac{1}{r})^2}{(ik + \frac{1}{r})^2 + \frac{1}{r^2}} \quad (27)$$

The formulas of the two equalizers will be converted into Laplace filters first by $s = i\omega$ and then into IIR digital filters by the bilinear transform $s = \frac{2}{T} \frac{z-1}{z+1}$. This process will be implemented in **Python**. The coefficients of the IIR digital filters will be fed into **Sigma studio** to achieve the equalization.

V Simulation & Experimental Result Analysis

In this section, the simulations and the experimental results are analyzed for the theoretical part covered in the previous section, and a brief description of the experimental configuration is given. Firstly, the rationality of the electromechanical model is verified by mechanical experiments; then the validity of the 2 equalizers is verified by measuring the membrane vibration velocities and the far-field sound pressure respectively; finally, the experimental results of 3D first-order directivity control of three shapes (omnidirectivity, cardioid, figure-of-eight) with three different aiming directions (on loudspeaker axis, on the system prism, and on the system corner) is illustrated.

V.1 Electromecanical behavior

In this study, the performance of the electromechanical characteristics of the system was divided into five settings, which are assigned in Table 1. They reflect the effect of the active speaker on itself as well as on the passive radiator when a single speaker is operating; the effect of the active speaker on itself as well as on the passive speaker when two facing speakers are operating out of phase; and the results when all speakers are moving in phase at the same time. The membrane velocities of the loudspeakers are measured and calculated by the displacement laser and the accelerometer, respectively (or only the accelerometer).

N#Configuration	N#working driver	N#observation driver	Dynamic response
1	Driver 3	Driver 3	$\frac{v_3}{U_3}$
2	Driver 3	Driver 6	$\frac{v_6}{U_3}$
3	Driver 5 and 6 (out of phase)	Driver 6	$\frac{v_6}{U_6}$
4	Driver 5 and 6 (out of phase)	Driver 1	$\frac{v_2}{U_6}$
5	All dirvers (in-phase)	Driver 1	$\frac{v_1}{U_1}$

Table 1: Configuration of electromechanical simulation and experimentation

The simulation and experimental results of Configuration 1 and 2 are presented in Figure 7. The simulation results are in general agreement with the experimental results. The results show that there are 2 peaks for both of the 2 configurations. The first peak corresponds to the resonant frequency of the loudspeaker according to the measured Thiele Small parameters. The presence of a second bump in the results with the enclosure indicates the effect of acoustic coupling between the drivers.

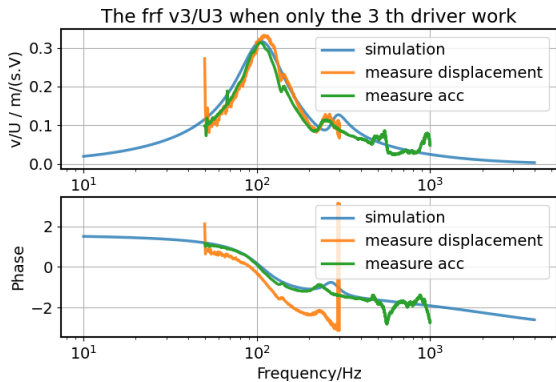
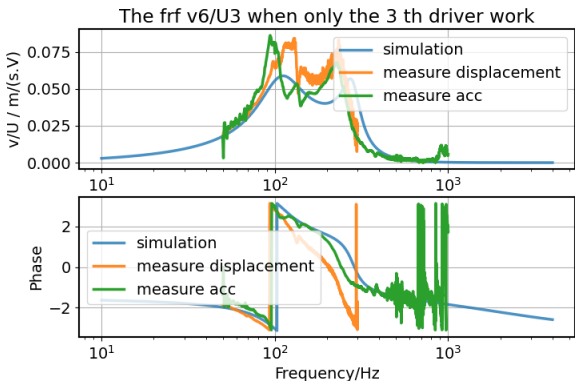

(a) Active dynamic transfer function $\frac{v_3}{U_3}$

(b) Passive dynamic transfer function $\frac{v_6}{U_3}$

Figure 7: Representation of simulation (blue curve) and experiment results (yellow and green curves) of active (left) and passive (right) dynamic transfer function $\frac{v_3}{U_3}$, $\frac{v_6}{U_3}$ when only the first driver works.

Figure 8 presents a validation simulation for a single driver. It compares its performance in a sealed box and in a compact hexahedron loudspeaker system with the same volume V_{abc} . The expansions of the motion equations of the two cases are the Equation (28), where the surface area of all membranes is assumed to be the same. By comparing the two equations, it can be seen that the change in the original first-order vibration system comes mainly from the passive vibration of other speakers.

$$G_1 v_{1s} + S_1^2 Z_{11}^- v_{1s} = \frac{Bl_1}{Z_{e_1}} U_{1s}; \quad G_1 v_{1c} + S^2 \sum_{l=1}^6 Z_{1l}^- v_{lc} = \frac{Bl_1}{Z_{e_1}} U_{1c}. \quad (28)$$

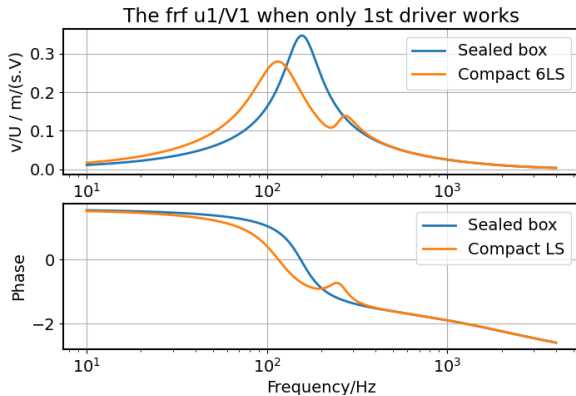


Figure 8: Representation of simulation results of the dynamic transfer function of the active loudspeakers mounted at the compact loudspeaker array system and at the same volume enclosure (only 1 driver working)

By manual calculation, the mathematical expressions for v_1/U_1 in the two cases are given by Equation (29), where $Z_{mbc} = \frac{S^2 \rho c^2}{j\omega V_{abc}}$ (the acoustic mass is neglected temporarily). The ratio of the two functions can be simplified to Equation (30). If the ratio approaches 1, the effect of acoustic coupling can be neglected, even when using a common enclosure. Based on the mathematical conclusion, the assumption is validated only when the ratio of the cavity volume to the square of the membrane area is sufficiently large while keeping other parameters constant. These two parameters also determine

the radiated power at low frequencies and the dispersion in different directions. It is necessary to find the appropriate volume of the enclosure and the appropriate surface area of the speaker to ensure that these three properties should be compensated.

$$\frac{v_{1s}}{U_{1s}} = \frac{Bl_1}{Ze_1(G_1 + Z_{mbc})}; \quad \frac{v_{1cn}}{U_{1cn}} = \frac{Bl_1[G_1 + 4Y_{mbc}]}{Ze_1G_1[G_1 + 5Z_{mbc}]}. \quad (29)$$

$$\frac{v_{1cn}}{U_{1cn}} \frac{U_{1s}}{v_{1s}} = 1 + \frac{4 \frac{Z_{mbc}}{G_1^2}}{1 + 5 \frac{Z_{mbc}}{G_1}}. \quad (30)$$

The simulation and experimental results of Configuration 3 and 4 are presented in Figure 9. The experimental results are consistent with the theoretical results. It can be seen that the second bump disappears when the two facing speakers start to move out of phase. In the condition of low frequency, using the knowledge of lumped element method, the acoustic coupling of the system can be seen as a one-dimensional acoustic mass, and the same conclusion can be derived from the previous theoretical model. Its effect on passive radiators in other directions is too small to constitute a second-order vibration system. Compared to the results of Configuration 2 (Figure 7b), the results of Configuration 4 (Figure 9b) show a very low magnitude and a lot of noise, which also supports the above point.

At high frequencies, especially after greater than 900 Hz, the experimental results of configuration 3 differ more from the simulation results, which is easier to observe from the phase. This is because when the frequency increases, standing waves are generated inside the box and resonance occurs. 900Hz is just the first cut-off frequency of the system. Therefore, the results of the system directivity control implementation will become worse with the increase in frequency.

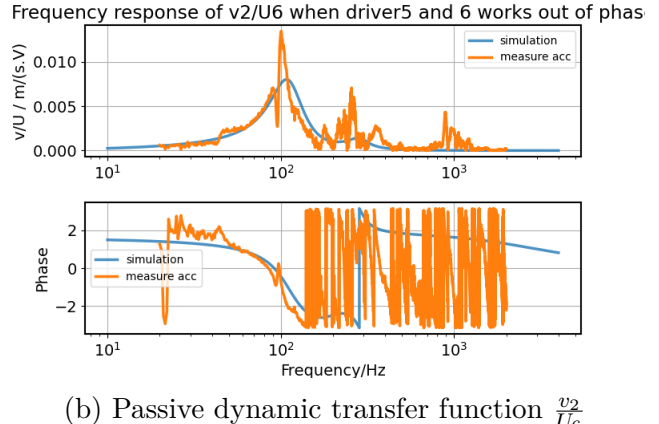
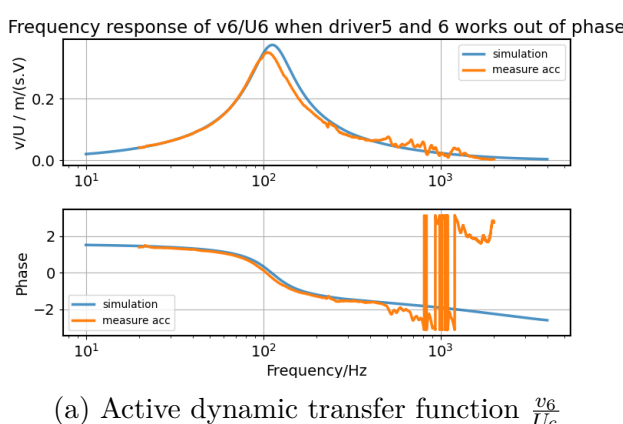


Figure 9: Representation of simulation (blue curve) and experiment results (yellow curve) of active (left) and passive (right) dynamic transfer function $\frac{v_6}{U_6}$, $\frac{v_2}{U_6}$ when drivers 5 and 6 work out of phase.

The simulation and experimental results when all drivers work in phase are presented in Figure 10. The resonant frequencies of both results are close to each other, which are higher than the resonant frequencies of speakers. Because when all drivers work together in phase, they can be seen as having their own smaller independent enclosures. However, the amplitude of the simulation result is bigger than the measurement result. With the Thiele Small parameters, the expression of the amplitude at the resonant frequency is Equation (31).

$$\frac{v_3}{U_3} = \frac{Bl_3}{Z_{e_3} \left(R_{ms3} + \frac{Bl_3^2}{Z_{e_3}} \right)} \quad (31)$$

From the expression, it can be found that the difference between the results comes from the inappropriate model of electrical impedance or mechanical viscosity model in higher frequencies (higher than the resonant frequency of the loudspeaker). The possibility of the viscosity model is lower because only one parameter can't change the amplitude of the peak and the mechanical quality, i.e. the sharpness of the peak at the same time. This means that the Thiele Small parameter model is not suitable for electromagnetic parameters at high frequencies. A better model is the Leach model [7], which considers the voice coil as a resistance, a lossy inductance, and a dependent voltage source. The parameters of this model will vary with the change of the frequencies. However, due to time constraints, the measurement and construction of such parametric models were not realized. The Thiele Small parameter is thus still retained and used.

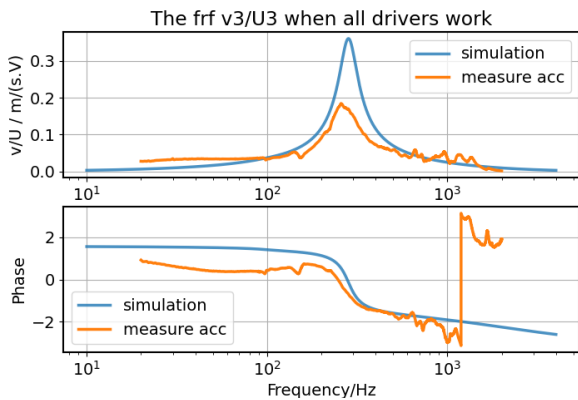


Figure 10: Representation of simulation (blue curve) and experiment results (yellow curve) of dynamic transfer function $\frac{v_3}{U_3}$ when all drivers works.

V.2 Validity of Heq

This subsection will demonstrate and analyze the feasibility of the equalizer. When all speakers are in phase at the same time and speakers 3 and 5 are out of phase working at the same input voltage, the measured vibration ratio of the membrane of driver3 is the experimental result of H_{eq13} . Its simulation and experimental results are represented in Figure 11. From the results, it can be seen that the simulated and experimental results in the range of [80,900] Hz match. The difference at about 300 Hz comes from the wrong model of the voice coil parameters when all drivers work in omnidirectional mode.

In the range of [20,80] Hz, the simulated results remain constant, but the experimental results gradually increase from near 0 dB. At low frequencies, it can be seen that only capacitance works in the system, and the expression for H_{eq1} can be simplified to Equation (32). During the experiment, one side of the system was always kept unsealed for ease of installation, which caused sound leakage in low frequencies when all speakers work. Therefore, the compression of sound in the internal intensity has less influence on the results, which means that the term in Equation (32) disappears at low frequencies. However, this assumption needs to be proved by advanced discussion and experiments. The operating range of the system is thus limited to bigger than 80 Hz.

$$H_{eq1lowF} = \frac{\frac{1}{j\omega C_{ms}} + 6S^2 Z_C}{\frac{1}{j\omega C_{ms}}}. \quad (32)$$

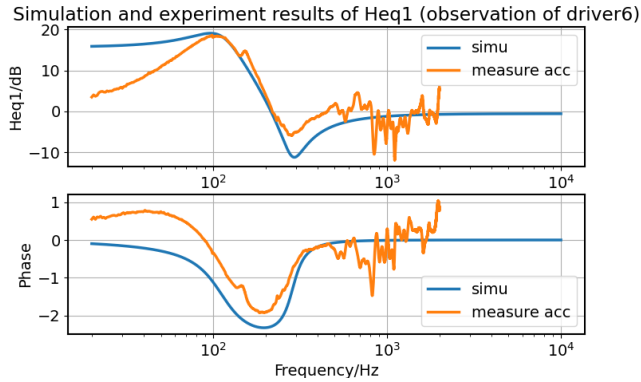


Figure 11: Representation of simulation (blue curve) and experiment (yellow curve) results of the first equalizer H_{eq1} of the third driver.

After adding H_{eq1} to the system, the measured results of H_{eq2} are shown in Figure 12. The experimental results showed similar trends to the simulation results. Since the aim of this study is to achieve directivity control, the differences between the simulated and experimental results can be accepted. However, for higher precision experimental studies, the results also need to be analyzed more deeply.

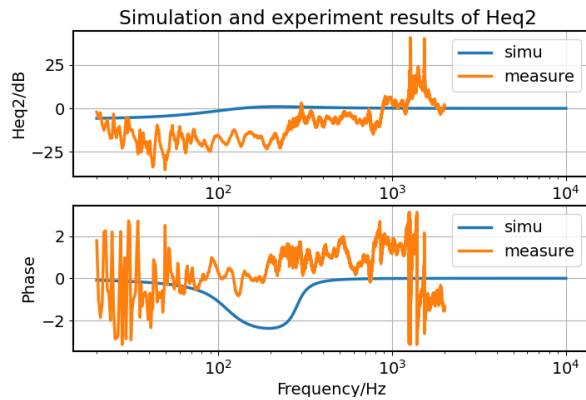


Figure 12: Representation of simulation (blue curve) and experiment (yellow curve) results of the first equalizer H_{eq2} .

V.3 Realization of 3D first-order beam control

This section focuses on the implementation and experimental validation of two key aspects of 3D first-order directivity control for a hexahedral loudspeaker array: first-order directivity shape change and aiming direction control.

V.3.1 Implement and DSP

As described in Section IV.3, 3D first-order directivity control can be achieved by independently controlling the input signals provided to the speakers at different locations. The input audio signal $s(t)$ to the system is decoded into a series of loudspeaker input signals through a matrix. Equation (25) gives the decoding matrix for the studied hexahedral loudspeaker array layout.

In addition, 3D first-order directivity control requires the loudspeaker array to have the same radiated sound pressure in both the monopole mode (six loudspeakers vibrating in phase) and the dipole mode (axial pairs of loudspeakers vibrating in opposite phase). In order to have the same radiated sound pressure in both modes, the monopole component of the loudspeaker signal must pass through a monopole-to-dipole equalizer. The calculation of the monopole-to-dipole equalizer is given in the theory Section IV.3.2.

According to the decoding matrix of the input signal to the loudspeakers given in Equation (25), the DSP design schema of the whole system is shown in Figure 13. Each speaker input signal is related to the loudspeaker position, directivity shape parameter α , and aiming direction (θ_0, ϕ_0) .

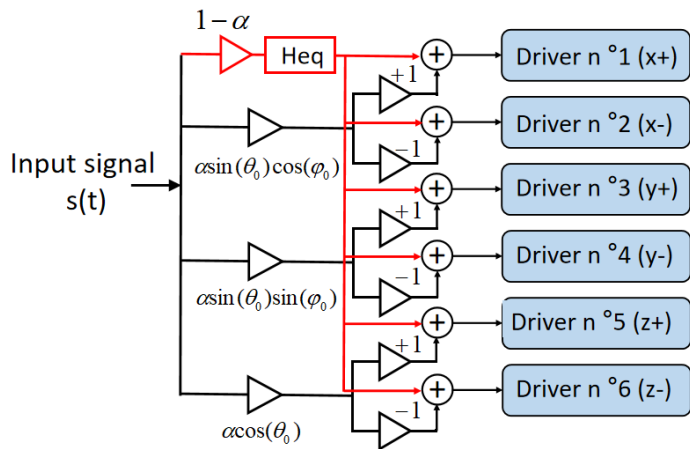


Figure 13: Representation of DSP schema for 3D first-order directivity control.

Equalizing the differences between the six drivers is also necessary to achieve better directivity control. Although six full-range speakers of the same model are used in this prototype, their actual measured TS parameters and sensitivity are slightly different. In order to make them equal, the monopole-to-dipole equalizer of each speaker is given according to the corresponding TS parameters, and each speaker is provided with the corresponding amplification compensation to make them have the same radiated sound efficiency.

In the calculation of the amplification compensation, speaker #2 with the lowest sensitivity is used as a reference, and the calculation formula is as follows:

$$A_i = 10^{\frac{L_{Mref} - L_{Mi}}{20}}, \quad (33)$$

Table 2 gives the measured sensitivity L_M of each speaker with the hexahedral enclosure at 1000 Hz, and the corresponding amplification compensation A_i calculation results.

N#driver	1 (x^+)	2 (x^-)	3 (y^+)	4 (y^-)	5 (z^+)	6 (z^-)
L_M [dB/W/m]	89.97	89.58	90.07	90.42	90.01	89.76
A_i	0.955	1	0.945	0.907	0.951	0.979

Table 2: Measured sensitivity of loudspeakers mounted on the cavity in 1000Hz and the corresponding amplification compensation.

In combination with the speaker signal processing described above, three dual-channel amplifier boards with integrated DSP are used to control the input voltage of each speaker independently. Figure 14 shows one of the DSP programs designed by Sigma Studio to control speakers #3 and #4 in the y-axis direction. The DSP program used to control the other two pairs of axially oriented speakers is essentially the same as the DSP program shown in Figure 14.

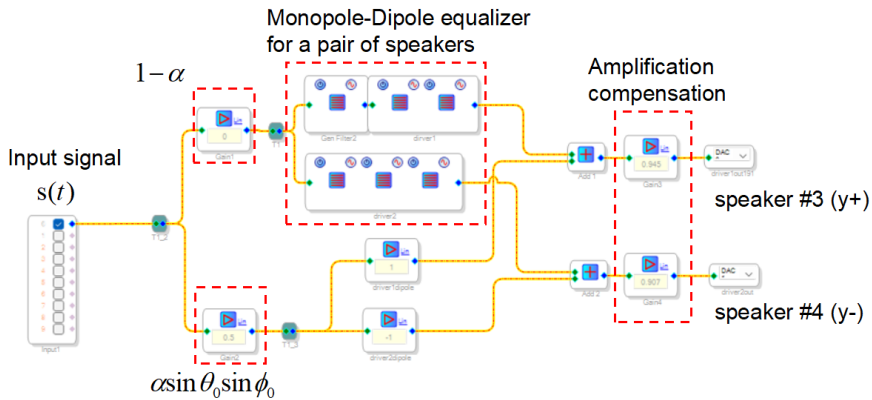


Figure 14: Representation of DSP program for speakers #3 and #4 in the y-axis direction.

V.3.2 Experimental setup

After completing the DSP setup and speaker system assembly, a series of directivity measurements were performed. The amplifier and other electronic systems were installed in a separate box from the loudspeaker array.

Directivity measurements in 3D space are obtained by measuring the radiated sound pressure over a far-field sphere centered on the loudspeaker array. To perform this measurement, a semicircular microphone stand with a radius of 0.5 m was fabricated. Figure 15 shows a diagram of the setup for the measurement experiment. The loudspeaker array was placed on a stand fixed to a turntable, the height of the stand and the position of the turntable ensured that the loudspeaker array was in the center of the semicircular microphone stand. And due to the limitations of the measurement equipment, the polar angles 0 and 180 degrees were not measured.

During the measurement, a chirp signal in the frequency band of 20 to 2000 Hz was sent to the system. 17 microphones were placed on the semi-circular stand at 10-degree intervals and a set of data was recorded for every 10-degree rotation of the turntable up to 360 degrees. Several directivity patterns at different frequencies were measured and the results were processed and presented with the help of **Python**.

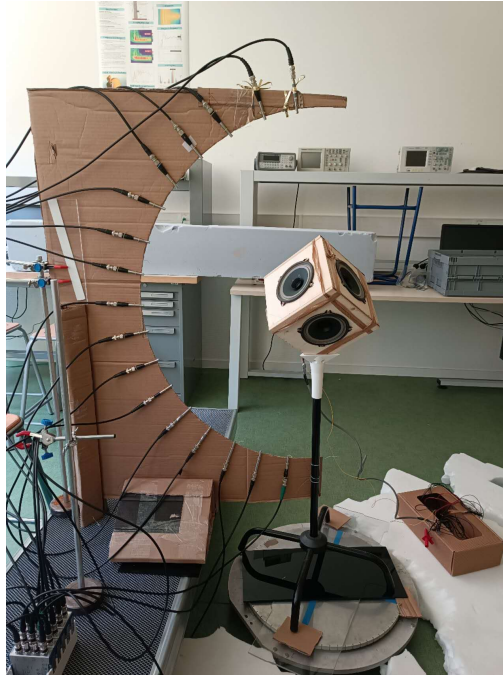


Figure 15: Photograph of the directivity measurement setup in 3D space.

V.3.3 Experimental results & Analysis

This subsection shows the measurement results of several directivity modes and the comparative analysis with the simulation results. The simulation results are plotted in Python, and its calculations are based on the radiated sound field calculations of the spherical cap model described in Subsection IV.2, combined with directivity control.

Since 3D directivity control is achieved by the weighted superposition of omnidirectional and bidirectional sound fields, the omnidirectional and bidirectional patterns of the loudspeaker array prototypes at different frequencies are shown and analyzed first. Figure 16 shows the simulation results and measurements of directivity for the omnidirectional pattern. The omnidirectional pattern corresponds to $\alpha = 0$ when all speakers vibrate in the same phase and the radiation pattern is independent of the aiming direction.

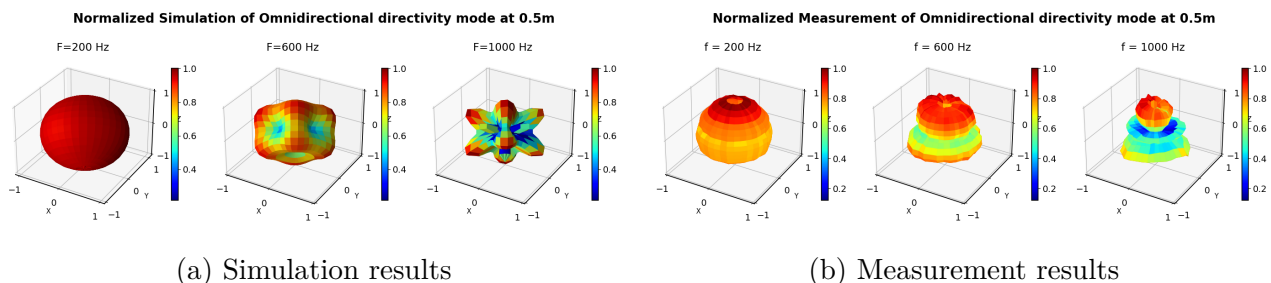


Figure 16: Representation of simulated and measured omnidirectional directivities at different frequencies.

As can be seen in Fig 16, at lower frequencies, the radiated sound field of the loudspeaker array can be considered approximately spherical. When the frequency is higher than 600Hz, the radiated sound field of the loudspeaker array starts to deform. Due to the limited number of loudspeakers

and coverage area of the vibrating membrane, the radiated sound field is close to square at 600 Hz. When the frequency continues to increase, the hexahedral loudspeaker array with much more complex directivity can no longer be used as an omnidirectional sound source.

Figure 17 shows the simulation results and measurements of the biaxiality pattern along the x-axis. Since the loudspeaker array was not placed horizontally on the stand at the time of measurement. The rotation matrix is used to rotate the experimental results 45° counterclockwise around the x-axis and 35.264° around the y-axis so that the presented results are consistent with the speaker pairs being parallel to the coordinate axes.

From Figure 17, the measurement results of the bidirectional mode agree well with the simulated results at low frequencies but converge to the quadratic radiation pattern around 1000Hz. This is because, at high frequencies, the internal action between the speakers of the common cavity is important. The vibration of the other passive membranes makes the overall radiation sound field show a quadripole. But the effective working range of the bidirectional pattern is still higher than the omnidirectional pattern, which can reach about 1000Hz.

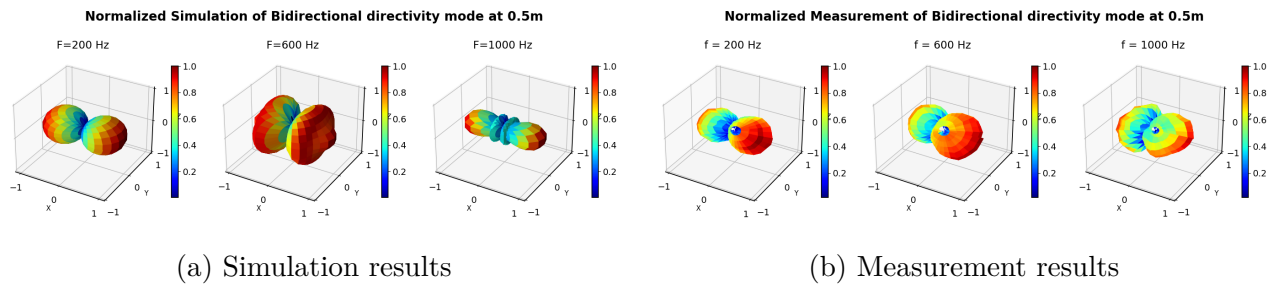


Figure 17: Representation of simulated and measured bidirectional directivities at different frequencies.

Figure 18 shows the simulated and measured results for the cardioid mode with different frequencies and with the aiming direction parallel to the x-axis. The measured results have some distortions but are still close to the simulated results. Since the cardioid mode is obtained by superimposing the omnidirectional radiated sound field and the bidirectional radiated sound field, it has a cutoff range between, around 800 Hz.

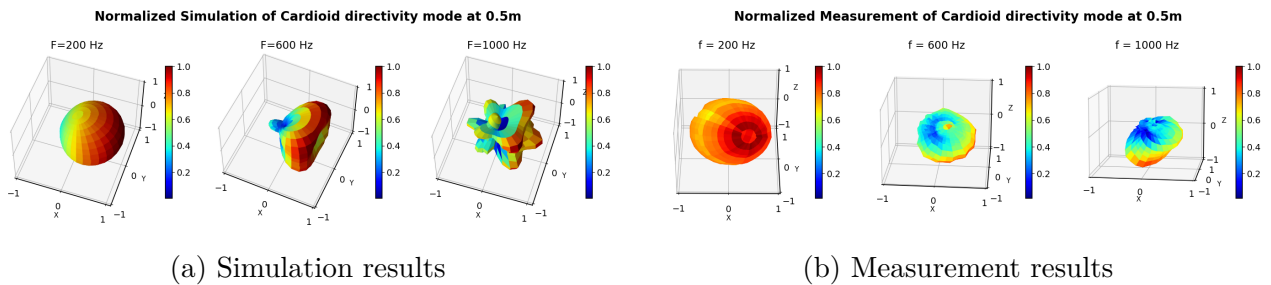


Figure 18: Representation of simulated and measured cardioid directivities at different frequencies.

To verify directivity control in 3D space, measurements for three sets of aiming directions are conducted: parallel to the x-axis, within the xy plane, and across the xyz space. These measurements are carried out for cardioid and figure-of-eight patterns, the measurement results and the corresponding

simulation results are presented in Figure 19. And all the related parameters for these measured directivity modes are shown in Table 3.

Mode	1	2	3	4	5	6
(θ_0, ϕ_0)	$(\frac{\pi}{2}, 0)$	$(\frac{\pi}{2}, 0)$	$(\frac{\pi}{2}, \frac{\pi}{4})$	$(\frac{\pi}{2}, \frac{\pi}{4})$	$(\frac{\pi}{4}, \frac{\pi}{4})$	$(\frac{\pi}{4}, \frac{\pi}{4})$
α	1	0.5	1	0.5	1	0.5
Shape	figure of eight	cardioid	figure of eight	cardioid	figure of eight	cardioid

Table 3: Measured 7 directivity modes and related parameters.

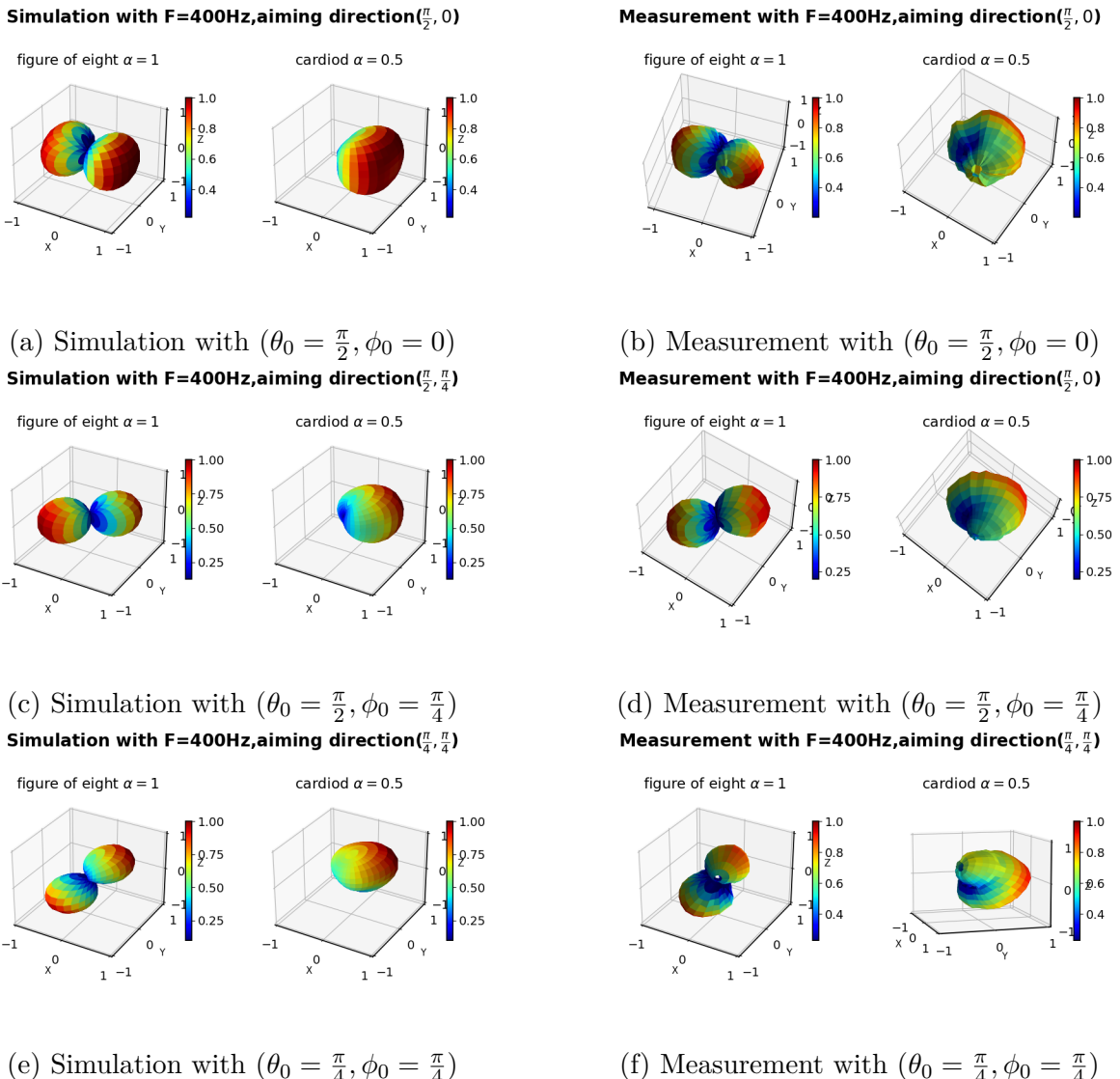


Figure 19: Representation of simulated and measured directivities with different aiming directions at 400 Hz.

As can be seen from the results in Figure 19, for all three aiming directions, the results of the figure-of-eight pattern match very well in shape and orientation with simulated results at 400 Hz, although it has a slight deflection relative to the simulated results due to measurement errors. The

measured sets of cardioid patterns are close to the simulated results, and the corresponding shapes and orientation can be barely seen, but the relative shifts and distortions are high.

VI Conclusion

In this project, a compact hexahedral loudspeaker array was successfully fabricated and its characteristics were investigated. The electromechanical model of the system can be constructed using experimentally estimated TS parameters and transmission line theory and acoustic analysis. Among them, the acoustic coupling of system speakers in different operating modes due to the presence of a common enclosure is the focus of modeling. The comparison of experimental and simulation results shows that the model fits well at low frequencies. However, the results of the system in the omnidirectional operation mode are different due to the limitation of the TS electrical parameters. A more rigorous Leach model should be used.

In order to achieve perfect beam control, two equalizers were used in the study to equalize the difference between the input monopole and dipole modes caused by the voltage when passing through the electromechanical system and the external field radiation. The validity of the two equalizers at low frequencies was verified experimentally. The first equalizer is generally correct but showed a bad consistency at very low frequencies, probably due to the sound leakage that occurs when the enclosure is not fully sealed. And the experimental and simulated results of the second equalizer differed considerably. The reasons for this problem may come from the influence of the measurement environment on the sound pressure, and the influence of the sound field generated by other working loudspeaker units on the observed sound field. The specific reasons need further exploration and practice. However, in general, the differences in equalizers are within the permissible limits of the achievable beam control.

The radiation model of each loudspeaker in the whole system is obtained by combining the boundary conditions and the spherical harmonic function. When the construction of the whole system is completed, beam control can be realized by changing the input signal. In this study, the construction of the beam control technique for the first-order 3D arbitrary direction is successfully completed. Experimental validation of the results was achieved with a 3D directional measurement device. The measurement results are similar to the experimental results and the 3D pointing can be observed. Although the system contains only 6 loudspeakers, it has been experimentally verified to be able to achieve beam control in three modes (omnidirectional, bidirectional, and unidirectional) at three positions (on loudspeaker axis, square prism, and square corner). Due to time constraints, the measurement results include only a fixed far-field distance. Directionality results for longer distances need to be continued.

In the future, this experimental model can continue to be used to study the possibilities of compact hexahedral loudspeaker arrays for sound field reproduction. To investigate whether it is possible to restore the sound field of a single instrument or multiple instruments, and more unknown applications.

Appendix

A Speaker Datasheet

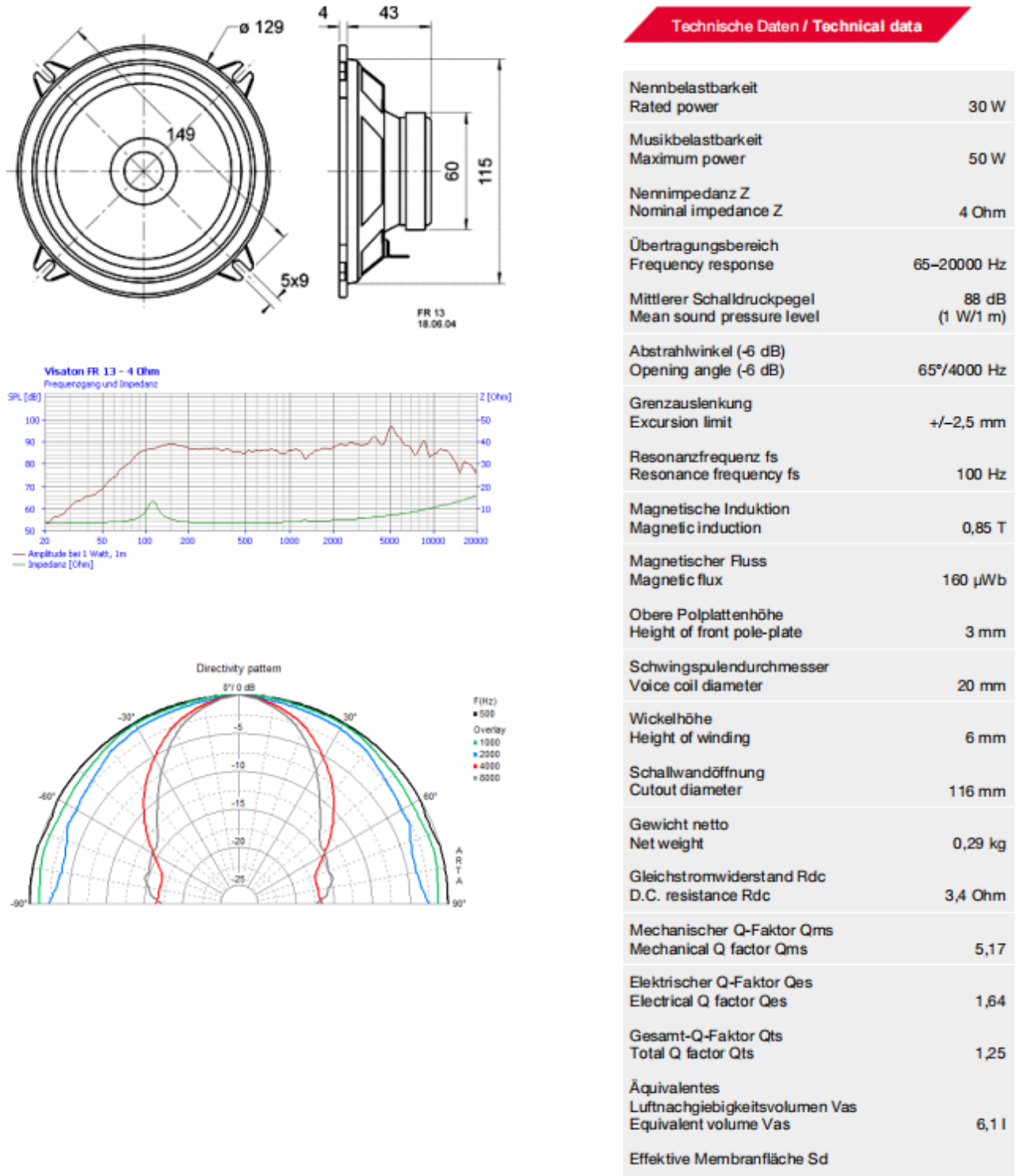


Figure 20: Datasheet of Visaton FR13-4 ohm full-range drivers

B Thiele & Small Parameters

N#driver	1	2	3	4	5	6
M_{ms}/g	3.68	3.59	3.25	3.63	3.12	3.76
V_{as}/L	5.57	5.78	7.16	6.01	6.93	5.45
$R_{ms}/kg/s$	0.360	0.318	0.330	0.320	0.308	0.317
$Bl/T.m$	2.28	2.09	2.02	2.13	1.95	2.17
R_e/Ω	3.83	3.66	3.69	3.57	3.77	3.63

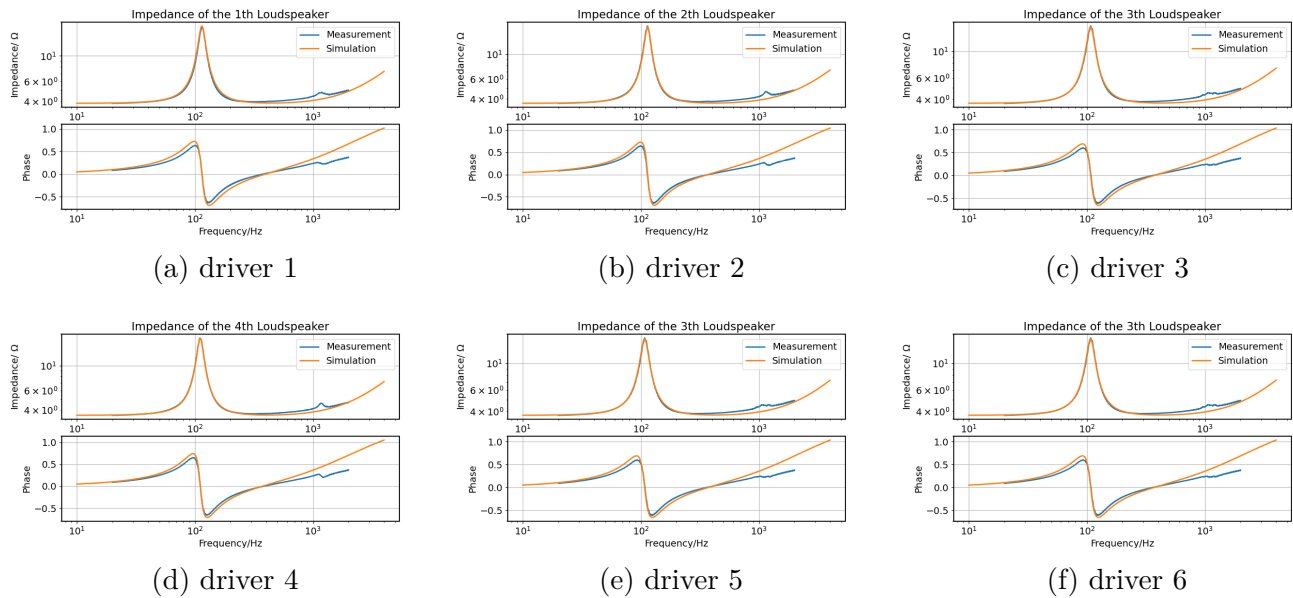


Figure 21: Measured electrical impedance curves and simulated curves of the six drivers.

C Derivation of the pressure expression in two dimention

The pressure expression of this 2D problem in harmonic is Equation (34). The walls are rigid at $x = 0$ and $x = L$, i.e. $\vec{v}|_{x=0} = \vec{v}|_{x=L} = 0$. By using the Euler equation and the two previous boundary conditions, the pressure expression is changed to Eq.35, where $k_{xm} = \frac{m\pi}{L}$. When $k_m > \frac{m\pi}{L}$, the corresponding waves appear. So before $k_1 = \frac{\pi}{L}$, there are only propagating waves in the y-axis, which corresponds to $f_1 \approx 900Hz$. Now the pressure expression below $f = 900Hz$ is Eq.36.

$$\hat{p}(x, y, \omega) = (\hat{A}\cos(k_x x) + \hat{B}\sin(k_x x)) (\hat{C}\cos(k_y y) + \hat{D}\sin(k_y y)). \quad (34)$$

$$\hat{p}(x, y, \omega) = \sum_{m=0}^{\infty} \hat{A}\cos(k_{xm} x) (\hat{C}\cos(k_y y) + \hat{D}\sin(k_y y)). \quad (35)$$

$$\hat{p}(x, y, \omega) = \hat{C}\cos(k_y y) + \hat{D}\sin(k_y y). \quad (36)$$

In the y -axis, the boundary conditions are $\vec{u}|_{y=0} = \vec{u}_4$ and $\vec{u}|_{y=L} = \vec{u}_3$. We also use the Euler equation twice more, the process is the Equation (37). After solving the two boundary condition equations, the expression of the coefficients \hat{C} and \hat{D} are Equation (38). It is thought that the pressure \hat{p}_1 obtained by membrane 1 can be simply considered the pressure at $y = \frac{L}{2}$, i.e. $\hat{p}(y = \frac{L}{2}, \omega)$. The final expressions of \hat{p}_1 are shown in Equation (39) and (40).

$$\begin{cases} \frac{\partial \hat{p}}{\partial y}|_{y=0} = -\frac{i\rho\omega}{S_m} u_4, \\ \frac{\partial \hat{p}}{\partial y}|_{y=L} = \frac{i\rho\omega}{S_m} u_3. \end{cases} \quad (37)$$

$$\begin{cases} \hat{C} = \frac{\hat{D}k\cos(kL) - i\rho\omega u_3}{ksinkL}, \\ \hat{D} = -\frac{i\rho\omega u_4}{k}. \end{cases} \quad (38)$$

$$\hat{p}_1\left(\frac{L}{2}, \omega\right) = \hat{C}\cos\left(k\frac{L}{2}\right) + \hat{D}\sin\left(k\frac{L}{2}\right). \quad (39)$$

$$\hat{p}_1\left(\frac{L}{2}, \omega\right) = -\frac{jZ_c}{2}\csc\left(\frac{kL}{2}\right)u_3 - \frac{jZ_c}{2}\csc\left(\frac{kL}{2}\right)u_4 = (Z_C - \frac{Z_M}{24})u_3 + (Z_C - \frac{Z_M}{24})u_4. \quad (40)$$

D Green's function + Integral formalism method

This appendix focuses on deriving the expression Z_a^- using the Green's function + Integral formalism method. The system depicted in Figure (22) (left) can be mathematically described. When only the l 'th loudspeaker is active, it can be modeled as a 3D square rigid system in length L with a moving piston at the boundary. To facilitate the analysis, a coordinate system is defined under the system, with the origin located at the center of the cavity as Figure (22) (right).

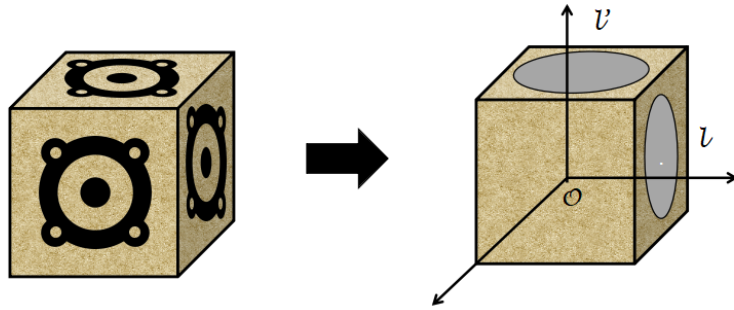


Figure 22: Sketch of system

The series expansion of the 3D Green's function can be written as the equation 41, where $\vec{r}_0 = (x_0, y_0, z_0)$ and $\vec{r} = (x, y, z)$ are the coordinates of the source and the coordinates of the observation point.

$$G(\vec{r}; \vec{r}_0) = \sum_i G_i(\vec{r}_0) \varphi_i^*(\vec{r}), \quad (i = (m, n, q), (x, y, z) \in \mathbb{R}), \quad (41)$$

$$\implies \lambda_i G_i(\vec{r}_0) = \varphi_i(\vec{r}_0) \implies G(\vec{r}; \vec{r}_0) = \sum_{i=0}^{\infty} \frac{\varphi_i(\vec{r}_0) \varphi_i^*(\vec{r})}{\lambda_i}. \quad (42)$$

For the cavity with rigid boundaries, i.e. Neumann condition, its eigenproblem can be expressed by the Helmholtz equation. Then combine the boundary conditions to obtain the solutions λ_i and φ_i (eigenvalue and eigenfunction). The i^{th} normalized eigenfunction and the eigenvalue λ_i is Equation 43 and Equation 44.

$$\varphi_i(x, y) = \sqrt{\frac{(2 - \delta_m^0)(2 - \delta_n^0)(2 - \delta_q^0)}{L^2}} \cos\left(\frac{m\pi}{L}x\right) \cos\left(\frac{n\pi}{L}y\right) \cos\left(\frac{q\pi}{L}z\right), \quad (43)$$

$$\lambda_i = \left(\left(\frac{m\pi}{L}\right)^2 + \left(\frac{n\pi}{L}\right)^2 + \left(\frac{q\pi}{L}\right)^2 - k^2 \right). \quad (44)$$

After preparing the all expressions, the Green's function of the cavity with rigid boundaries is shown as follow :

$$G(\vec{r}; \vec{r}_0) = \sum_{(m,n,q)} \sqrt{\frac{(2 - \delta_m^0)(2 - \delta_n^0)(2 - \delta_q^0)}{L^2}} \frac{\cos(\frac{m\pi}{L}x)\cos(\frac{n\pi}{L}y)\cos(\frac{q\pi}{L}z)\cos(\frac{m\pi}{L}x_0)\cos(\frac{n\pi}{L}y_0)\cos(\frac{q\pi}{L}z_0)}{k_m^2 + k_n^2 + k_q^2 - k^2}. \quad (45)$$

Where the expression of $f(\vec{r})$ with the convention $e^{j\omega t}$ is the equation 46. Here we think the source is a constant volume velocity source which is placed at \vec{r}_0 with the volume velocity is $q = Q_0 e^{j\omega t}$.

$$f(\vec{r}) = \rho_0 \left(\operatorname{div}(\vec{F}) - \frac{\partial q}{\partial t} \right) = -i\rho_0\omega Q_0 \delta(x - x_0)\delta(y - y_0)\delta(z - z_0). \quad (46)$$

By applying the Integral formalism, the acoustic field distribution inside the cavity induced by the l' th loudspeaker can be expressed. Knowing that there is no source in the cavity. The approximated boundary condition of the Green's function is Neumann condition. Hence the first and the third term can be cancelled. The acoustic field obtained is as follow :

$$p(\vec{r}, \omega) = \int_{L/2}^{L/2} \int_{L/2}^{L/2} \int_{L/2}^{L/2} f(\vec{r}_0) G(\vec{r}; \vec{r}_0) dx_0 dy_0 dz_0 + \int \int_{S_{l'}} \left(G(\vec{r}; \vec{r}_0) \partial_{n_0} p(\vec{r}_0) - \underline{p(\vec{r}_0) \partial_{n_0} G(\vec{r}; \vec{r}_0)} \right) dS_0, \quad (47)$$

$$\hat{p}(\vec{r}, \omega) = i\omega\rho V_0 \sum_{(m,n,q)} (-1)^n \sqrt{\frac{(2 - \delta_m^0)(2 - \delta_n^0)(2 - \delta_q^0)}{k_m^2 + k_n^2 + k_q^2 - k^2}} \cos\left(\frac{m\pi}{L}x\right) \cos\left(\frac{n\pi}{L}y\right) \cos\left(\frac{q\pi}{L}z\right) \int \int_{S_{l'}} \cos\left(\frac{m\pi}{L}x_0\right) \cos\left(\frac{n\pi}{L}y_0\right) \cos\left(\frac{q\pi}{L}z_0\right) dS_0.$$

The average pressure received by the l th membrane is obtained by integrating the pressure on its surface and dividing it by the membrane area. It is assumed that the volume velocity provided by the moving piston is the same for the whole internal space of the cavity. The internal acoustic impedance of the l th loudspeaker fed by the vibration of the l' th loudspeaker is Equation 48.

$$Z_{ll'}^- = \frac{\int \int_{S_l} \hat{p}(\vec{r}, \omega) dS_0}{S_l S_{l'} v_{l'}}. \quad (48)$$

References

- [1] A.M.Pasqual, P.Herzog, and J.R.Arruda, “Theoretical and experimental analysis of the electromechanical behavior of a compact spherical loudspeaker array for directivity control,” *The Journal of the Acoustical Society of America*.
- [2] A.M.Pasqual, “Spherical harmonic analysis of the sound radiation from omnidirectional loudspeaker arrays,” *Journal of Sound and Vibration*, 2014.
- [3] T. Deppisch, N. Meyer-Kahlen, F. Zotter, M. Frank, “Surround with Depth on First-Order Beam-Controlling Loudspeakers ,” *Audio Engineering Society Convention Paper 9977*, p. 4, 2018.
- [4] F.Zotter, M.Frank, “Ambisonics, A Practical 3D Audio Theory for Recording, Studio Production, Sound Reinforcement, and Virtual Reality,” *Springer Topics in Signal Processing*.
- [5] Jean-Pierre Dalmont, “Line theory appliedto acoustics ,” *Transmission line tutorial*, pp. 23–27, 2021.
- [6] S.Raetz, “The pulsating sphere, notion of monopole ,” *Radiation elements tutorial*, p. 87, 2021.
- [7] W. Marshall Leach, “Loudspeaker Voice-Coil Inductance Losses: Circuit Models, Parameter Estimation, and Effect on Frequency Response,” *JOURNAL OF THE AUDIO ENGINEERING SOCIETY*, 2002.